Frequency Regulation of VSC-MTDC System with Offshore Wind Farms

Haoyu Liu and Chongru Liu, *Senior Member*, *IEEE*

***Abstract*—Frequency regulation of voltage source converter-based multi-terminal high-voltage direct current (VSC-MTDC) system with offshore wind farms enhances the frequency stability by compensating the power for a disturbed AC system. However, it is difficult to reasonably allocate frequency-regulation resources due to a lack of coordination mechanisms between wind farms and the MTDC system. Moreover, it is difficult for the frequency control of the wind farms to manage changes in wind speed; and the risk of wind-turbine stalls is high. Thus, based on the kinetic energy of wind turbines and the power margin of the converters, the frequency-regulation capability of wind turbines is evaluated, and a dynamic frequency-support scheme considering the real-time frequency-support capability of the wind turbines and system frequency evolution is proposed to improve the frequency-support performance. A power adaptation technique at variable wind speeds is developed; the active power in the frequency-support stage and restoration stage is switched according to the wind speed. A hierarchical zoning frequency-regulation scheme is designed to use the frequency-regulation resources of different links in the MTDC system with wind farms. The simulation results show that the novel frequency-regulation strategy maintains frequency stability with wind-speed changes and avoids multiple frequency dips.**

***Index Terms*—Wind generation, voltage source converter-based multi-terminal high-voltage direct current (VSC-MTDC), frequency regulation, cooperative control, adaptive control, variable wind speed.**

I. Introduction

LARGE-SCALE offshore wind-power bases meet the demands of energy development [1]. With its flexible operation modes, a voltage source converter based multi-terminal high-voltage direct current (VSC-MTDC) system is an essential means of transmitting offshore wind power [2]. However, permanent magnet synchronous generators (PMSGs) operate in maximum power point tracking (MPPT) mode [3] and are isolated by DC grids and back-to-back converters, which makes them incapable of responding to the frequency disturbances of AC systems [4]. Thus, it is critical to investigate the auxiliary frequency-regulation strategy of VSC-MTDC system with offshore wind farms to enhance the frequency stability of AC systems [5].

Wind-turbine (WT) frequency regulation is divided into two stages: frequency support and restoration. To develop the frequency-support capability of the WT, overspeed control [6], [7], pitch angle control [8], [9], virtual synchronous generator control [10], [11], and virtual inertia integrated control (VIIC) [12]-[17] have been proposed. Under normal conditions, the VIIC operates in MPPT mode, releasing the kinetic energy of the WT rotor to provide power support in the frequency-support stage by emulating the inertia and damping of the synchronous generators. VIIC has a distinct physical meaning, which does not affect the economic operation of the WT, and is widely used.

Nevertheless, traditional VIIC uses fixed coefficients [12], resulting in poor operational flexibility. Minor gains are ineffective for frequency regulation, whereas large gains improve the frequency nadir but may cause the wind turbines to stall. Thus, a time-varying proportional coefficient [13], [14] has been designed to enhance WT frequency-regulation performance. To reflect the WT status, [15] adds the rotational speed margin to the time-varying coefficient [13], [14]. Reference [16] uses the rotor motion equation of a WT and the system frequency state to calculate the real-time equivalent inertia coefficient. The damping coefficient is dynamically adjusted in accordance with the frequency excursions (FEs) and rate of change of frequency (ROCOF), which characterize the system frequency state [17]. The rotational speed and kinetic energy margins of the WT, which indicate the rotational-speed state of the WT, are introduced into the damping coefficients [18], [19]. References [20] and [21] include the kinetic energy margin of the WT in the inertia and damping coefficients. Reference [22] applies a frequency deviation into the MPPT module, provides inertial support by running the WT with a suboptimal solution, and introduces a frequency differential into the virtual inertia coefficient to accelerate the frequency response. However, these enhanced solutions have not considered the severity of the frequency disturbances or the real-time frequency-regulation capability of the WT.

Several of the aforementioned solutions to frequency support make use of the rotational speed margin [15], [18] and kinetic energy margin [19]-[21] to reflect the frequency-regulation capacity of the WT. However, the frequency-regulation potential of a WT is affected by circumstances other

Manuscript received: January 3, 2023; revised: February 12, 2023; accepted: April 11, 2023. Date of CrossCheck: April 11, 2023. Date of online publication: May 19, 2023.

This work was supported by the National Key R&D Program of China (No. 2022YFB2402700).

This article is distributed under the terms of the Creative Commons Attribution 4.0 International License (http://creativecommons.org/licenses/by/4.0/).

H. Liu and C. Liu (corresponding author) are with North China Electric Power University, Beijing 102206, China (e-mail: haoyu_l@126. com; chongru. liu@ncepu.edu.cn).

DOI: 10.35833/MPCE.2023.000001

than its operational state. Thus, it is important to develop a more appropriate approach for evaluating the frequency-regulation potential of a WT.

After the frequency-support stage, the WT usually starts to restore the rotational speed to avoid uneconomical low rotational speed operation, resulting in a second frequency dip (SFD) and threatening the safety of the power system [11]. Energy-storage strategies [23], [24] and initiative power control [21], [25]-[29] have been proposed to avoid an SFD. Energy-storage strategies use energy-storage devices to compensate for power shortages during the restoration stage. If the energy-storage capacity is sufficient, the SFD is eliminated, which is beneficial for balancing WT power fluctuation during normal operations. However, adequate energy storage requires significant investment. To reduce the SFD without further investment, the initiative power control must tweak existing control links and adjust the electromagnetic power of the WT during the restoration stage.

The VIIC and initiative power control complete the frequency support and rotational speed recovery of the WT; however, these strategies are confined to a single wind speed, lacking the ability to manage the changes of wind speed.

Modular multilevel converter (MMC) is one of the most popular forms of offshore wind power transmission; it has become an important issue to exploit the cooperative frequency regulation potential of MMCs and offshore wind farms [11]. Based on WT frequency-regulation strategies [12]-[22], [25]-[29], the auxiliary frequency control of onshore and offshore VSCs [16], [21], [30], [31] has been developed to implement frequency regulation of wind farms via a single MMC-HVDC system. To enhance the frequency stability of AC systems, frequency-response control schemes for wind farms using the VSC-MTDC system have been suggested [1], [4], [32], [33]. Under this setting, all wind farms engage in frequency regulation in the event of an active power imbalance, regardless of the severity of the frequency disturbance. Frequent power disturbances in AC systems make it easier for WTs to break the MPPT mode, which drastically reduces WT operating efficiency. Rational allocation of the frequency-regulation sequence of wind farms and onshore VSCs significantly enhances frequency-regulation performance.

The difficulties in achieving satisfactory frequency-regulation performance in MTDC system with wind farms lie in three areas: ① balancing the system frequency evolution and real-time frequency-regulation capacity of the WT during the frequency-regulation stage; ② managing wind-speed variation during the frequency-support and restoration stages; ③ coordinating wind farms and onshore VSCs for cost-effective operation and reduction of multiple frequency dips.

To address these problems, a novel cooperative frequency-regulation scheme for a VSC-MTDC system with wind farms is proposed. The main contributions of this paper are presented as follows.

1) A novel approach to evaluating WT frequency-regulation capacity is developed, and an adaptive WT frequency-support approach is suggested in combination with a frequency-regulation capacity factor. In this context, the WT support power is adjusted dynamically according to the real-time frequency-regulation capacity and the frequency evolution of the offshore AC system to optimize the frequency-regulation performance.

2) A WT power adaptation technique at variable wind speeds is proposed. During the frequency-support stage, a fundamental power reference tuning approach is developed to cooperate with the power buffer interval and strike a balance between frequency support and SFD reduction. A linear power transition approach is proposed to adapt to the changes of wind speed during the restoration stage.

3) A hierarchical zoning frequency-regulation scheme for an MTDC system with wind farms is suggested to weaken multiple frequency dips and guarantee frequency-regulation performance. Wind farms in MTDC systems are divided into two types based on their frequency-regulation capabilities. Furthermore, a stepped frequency-regulation framework is developed for generators in disturbed AC systems, DC capacitors, wind farms, and normal AC systems.

The remainder of this paper is organized as follows. Section II introduces the control of VSC-MTDC system with wind farms. A cooperative frequency-regulation scheme is proposed in Section III. Simulations are conducted in Section IV to validate the novel frequency-regulation scheme. Section V concludes this paper.

II. Control of VSC-MTDC System with Wind Farms

Figure 1 depicts the topology of VSC-MTDC system with offshore wind farms and the control system. The DC grid uses a mesh topology to demonstrate universality.

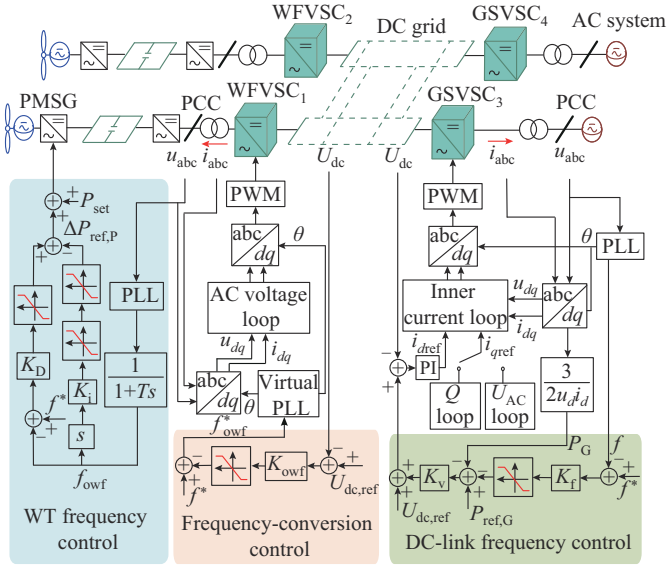

Fig. 1. Topology of VSC-MTDC system with offshore wind farms and control system.

In Fig. 1, GSVSCs indicate VSCs connected to onshore AC systems and WFVSCs denote VSCs connected to offshore wind farms; PCC represents the point of common cou-

pling; PLL represents the phase-lock loop; PWM represents the pulse-width modulation; and PI represents the proportional-integral controller. K_v and K_f are the DC voltage and frequency droop coefficients, respectively; f^* and f are the reference and actual AC system frequencies, respectively; $P_{ref,G}$ and $U_{dc,ref}$ are the active power and DC voltage reference values of the GSVSC, respectively; P_G and U_{dc} are the actual active power and DC voltage, respectively; f_{owf} and f^*_{owf} are the frequency of an offshore AC system and its reference value, respectively (normally, $f^*_{owf}=f^*$); K_{owf} is the frequency-conversion coefficient of the WFVSC; $\Delta U_{dc}=U_{dc,ref}-U_{dc}$; $\Delta f=f^*-f_{owf}$; $\Delta P_{ref,P}$ is the power reference increase generated by the VIIC; P_{set} is the basic power of the PMSG, which is normally equal to the power command of the MPPT module P_{MPPT}; K_D and K_i are the equivalent damping and inertia coefficients, respectively; u_{abc} and i_{abc} are the AC voltage and current of the PCC, respectively; and u_{dq} and i_{dq} are the dq-axis components of the AC voltage and current of the PCC, respectively.

All VSCs and PMSGs have used dual closed-loop vector control. The outer loop control of the GSVSC is uniformly expressed using a droop control. An additional frequency control [33] couples the AC system frequency with the active power and DC voltage of the GSVSC; and the FE uses droop control to transmit unbalanced power to the DC grid. Thus, the active power control of the GSVSC is expressed as:

$$P_{ref,G}-P_G=-\frac{1}{K_v}(U_{dc,ref}-U_{dc})+K_f(f^*-f) \tag{1}$$

The WFVSC uses a fixed AC voltage and frequency control to harness the active power of the wind farms. Fixed-frequency control uses a virtual PLL to generate the reference frequency for offshore AC systems. Frequency-conversion control [11] converts the DC voltage deviation into the FE of the WFVSC and serves as the foundation for offshore wind farms to participate in system frequency regulation.

$$f_{owf}=f^*_{owf}=f^*-K_{owf}(U_{dc,ref}-U_{dc}) \tag{2}$$

Normally, the machine-side converter of a PMSG uses a fixed active power control, and the power command is generated by the MPPT module. For frequency support of a wind farm, VIIC [12] adds a frequency-response component to the MPPT power command.

$$P_{ref,P}=P_{set}+\Delta P_{ref,P} \tag{3}$$

where $P_{ref,P}$ is the active power reference for the PMSG. $\Delta P_{ref,P}$ is expressed as:

$$\Delta P_{ref,P}=K_D\Delta f-K_i\frac{df_{owf}}{dt} \tag{4}$$

According to (3) and (4), under the action of VIIC, when f_{owf} changes, the WT uses the kinetic energy of the rotor to generate active power for fast frequency support.

The synergy of these controls transmits frequency disturbances from the grid side to the source side, facilitates frequency support from the source side to the grid side, and improves the frequency stability of disturbed AC systems.

III. Cooperative Frequency-regulation Scheme

A coordinated frequency-regulation scheme for VSC-MTDC system with offshore wind farms is proposed to address the poor flexibility of the VIIC with fixed proportional coefficients and the inability to manage the changes of wind speed. Section III-A introduces a novel evaluation approach to WT frequency regulation. The frequency-support and rotational speed recovery schemes of the WT are discussed in Section III-B and III-C, respectively. Section III-D describes how wind farms cooperate with other modules in the MTDC system. Small-signal stability is analyzed in Section III-E.

A. Evaluation Approach to WT Frequency Regulation

The available frequency-support resources when a WT regulates the frequency are determined by the amount of releasable rotor kinetic energy. Thus, the releasable kinetic energy margin has been primarily used to evaluate the frequency-regulation capacity of the WT [25].

$$G_{C,1}=\frac{E_{k,0}-E_{k,min}}{E_{k,max}-E_{k,min}}=\frac{H\omega^2_{r,0}-H\omega^2_{r,min}}{H\omega^2_{r,max}-H\omega^2_{r,min}}=\frac{\omega^2_{r,0}-\omega^2_{r,min}}{\omega^2_{r,max}-\omega^2_{r,min}} \tag{5}$$

where $G_{C,1}$ is the classical frequency-regulation capacity of the WT; H is the inertia time constant; $E_{k,0}$, $E_{k,max}$, and $E_{k,min}$ are the initial, maximum, and minimum rotor kinetic energies of the WT, respectively; and $\omega_{r,0}$, $\omega_{r,max}$, and $\omega_{r,min}$ are the initial, maximum, and minimum WT rotational speeds, respectively.

The traditional evaluation approach only considers the WT state; however, the actual frequency-regulation power transmitted from the WT to the PCC is restricted by the WT state and the power margin of the back-to-back converters. Because frequency support relies heavily on additional active power, the closer the initial active power is to the power limit, the less room there is for auxiliary power for frequency regulation.

Considering this issue, a novel WT frequency-regulation capacity factor $G_{C,2}$ is proposed in conjunction with the releasable kinetic energy and power margins.

$$G_{C,2}=\frac{\omega^2_{r,0}-\omega^2_{r,min}}{\omega^2_{r,max}-\omega^2_{r,min}}\frac{P_{max}-P_0}{P_{max}-P_{min}} \tag{6}$$

where P_0 is the initial power of the WT; and P_{max} and P_{min} are the maximum and minimum power of the PMSG converters, respectively.

P_0 from the MPPT module [3] is substituted into (5) and (6) to calculate $G_{C,1}$ and $G_{C,2}$. The calculation results of frequency regulation capacity coefficients of PMSG after normalization are shown in Fig. 2.

In Fig. 2, $G_{C,1}$ gradually increases as $\omega_{r,0}$ increases. However, when $\omega_{r,0}$ increases, $G_{C,2}$, which considers the power margin of the converters, tends to increase and then decrease. This demonstrates that when $\omega_{r,0}$ is small, the power margin of the converters is sufficient and the power of the WT is fully transmitted to the WFVSC. The kinetic energy of the rotor that can be released is the dominant factor in the frequency-regulation capacity of the WT. Although the released kinetic energy of the WT continues to increase as $\omega_{r,0}$ in-

creases, the output power of the WT approaches the power limit of the converters, and the frequency-regulation capacity of the WT gradually decreases. $G_{C,2}$ accurately represents the real-time frequency-regulation capacity of the WT.

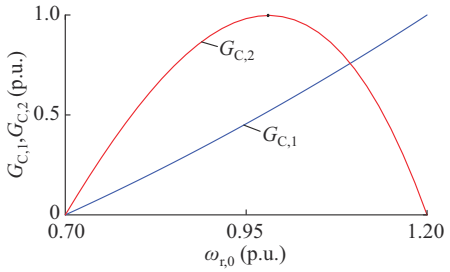

Fig. 2. Calculation results of frequency-regulation capacity coefficients of PMSG after mormalization.

The frequency-regulation capacity of a WT is defined in (6). The frequency-regulation capacity of the entire wind farm is estimated using the average kinetic energy approach [34].

$$G_{C,WF}=\frac{\sum_{i=1}^{n}G_{C,2,i}(\omega_{r,max,i}^2-\omega_{r,min,i}^2)}{\sum_{i=1}^{n}(\omega_{r,max,i}^2-\omega_{r,min,i}^2)} \tag{7}$$

where $G_{C,WF}$ is the frequency-regulation capacity of a wind farm; $G_{C,2,i}$ is the frequency-regulation capacity factor of WT$_i$; and n is the number of WTs in the wind farm.

An approach to evaluating the frequency-regulation capacity of a WT and an entire wind farm has been proposed considering both the WT operating state and the power margin of the converters. It serves as a theoretical foundation for the adaptive frequency-support scheme of the WT and the hierarchical zoning frequency-regulation scheme of the VSC-MTDC system.

B. Adaptive Frequency-support Scheme of WT

1) Adaptive Frequency-support Coefficients

Equivalent damping and inertia coefficients of the VIIC are fixed, resulting in poor adaptation to frequency disturbances of varying severity. Thus, with the frequency-regulation capacity in (6) and the real-time evolution of the frequency disturbance, adaptive K_D and K_i are designed to satisfy the requirements of frequency regulation. Under this setting, given that WT power-reduction approaches are mature [6]-[9], this paper focuses on the frequency drops in AC systems that require the WT to increase output power.

$\mathrm{d}f_{owf}/\mathrm{d}t$ is relatively large in the early stages of a frequency disturbance. The equivalent inertia control plays a major role. Considering the real-time frequency-regulation capacity of the WT, K_i is set as a function of $G_{C,2}$ and $\mathrm{d}f_{owf}/\mathrm{d}t$ to ensure the early frequency-regulation performance of the WT. As Δf gradually increases over time and the equivalent damping control becomes the dominant force of the VIIC, K_D is set as a function of $G_{C,2}$ and Δf to ensure that the WT has sufficient frequency-regulation capacity in the later stage of frequency regulation.

K_i is defined as:

$$K_i=K_{i0}G_{C,2}g_i \tag{8}$$

where K_{i0} is the fundamental inertia coefficient. Unlike (6), which only considers the initial power P_0, the real-time power P of the WT is used to calculate $G_{C,2}$ in (8).

$$G_{C,2}=\frac{\omega_r^2-\omega_{r,min}^2}{\omega_{r,max}^2-\omega_{r,min}^2}\frac{P_{max}-P}{P_{max}-P_{min}} \tag{9}$$

g_i is defined as:

$$g_i=\begin{cases}\dfrac{g_{i0}}{\left.\dfrac{\mathrm{d}f_{owf}}{\mathrm{d}t}\right|_{t=0}}\dfrac{\mathrm{d}f_{owf}}{\mathrm{d}t} & \dfrac{\mathrm{d}f_{owf}}{\mathrm{d}t}<0\\ 0 & \dfrac{\mathrm{d}f_{owf}}{\mathrm{d}t}\geq 0\end{cases} \tag{10}$$

where g_{i0} is the initial value of g_i.

$G_{C,2}$ is the real-time frequency-regulation capacity of the WT. The greater $G_{C,2}$ and K_i, the more inertial support the WT can provide. Moreover, g_i reflects the development of frequency disturbances. The larger $\mathrm{d}f_{owf}/\mathrm{d}t$ and g_i, the more significant the inertial control. As $\mathrm{d}f_{owf}/\mathrm{d}t$ decreases to zero or increases in the opposite direction, the inertial control has a negative effect on frequency regulation. We set g_i to zero to eliminate negative effects.

K_D is defined as:

$$K_D=K_{D0}G_{C,2}g_D \tag{11}$$

where K_{D0} is the basic damping coefficient. g_D is defined as:

$$g_D=\begin{cases}g_{D0}+\alpha\Delta f & \dfrac{\mathrm{d}f_{owf}}{\mathrm{d}t}<0\\ g_{D0}+\alpha\Delta f_{max} & \dfrac{\mathrm{d}f_{owf}}{\mathrm{d}t}\geq 0\end{cases} \tag{12}$$

where g_{D0} is the initial value of g_D; and α is the scale gain. When $\mathrm{d}f_{owf}/\mathrm{d}t$ is equal to 0, Δf reaches its maximum value Δf_{max}. The analytical approach [35] and predictive approach [36] are used to compute the frequency nadir, and its maximum value is used to obtain Δf_{max}, which is expressed as:

$$\Delta f_{max}=\max(\Delta f_{max,a},\Delta f_{max,p}) \tag{13}$$

where $\Delta f_{max,a}$ and $\Delta f_{max,p}$ are the frequency nadirs obtained by the analytical and predictive approaches, respectively.

Similar to K_i, K_D is also affected by $G_{C,2}$ and g_D. g_D increases gradually with the increase of Δf, and the effect of the damping control on frequency support is strengthened. Figure 3 shows diagrams of K_i, K_D, and $\Delta P_{ref,P}$.

When a frequency disturbance occurs, ω_r and f do not change significantly at first, although $\mathrm{d}f/\mathrm{d}t$ is relatively large. This leads to a higher K_i. $\Delta P_{ref,P}$ increases rapidly under the action of K_i, providing fast and sufficient power support. With the progress of frequency support, although K_D remains high, the kinetic energy of the WT is gradually released, and its frequency-regulation capacity is weakened. Thus, $\Delta P_{ref,P}$ decreases as ω_r decreases to prevent excessive frequency support from threatening safe operation of the WT.

2) Basic Power Tuning Approach with Variable Wind Speeds

As indicated in (3), $P_{ref,P}$ includes two parts: the fundamental reference power P_{set} and the additional power $\Delta P_{ref,P}$. To ensure that the WT output power is always larger than $P_{MPPT}(\omega_{r,0})$ during the frequency-support stage, P_{set} is typical-

ly set as the initial power $P_{\mathrm{MPPT}}(\omega_{\mathrm{r},0})$ [37].

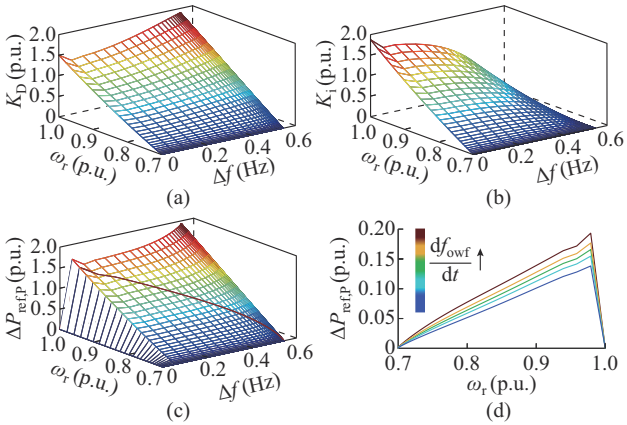

Fig. 3. Adaptive frequency-regulation coefficients. (a) K_{D}. (b) K_{I}. (c) $\Delta P_{\mathrm{ref,P}}$ represented by ω_{r} and Δf. (d) $\Delta P_{\mathrm{ref,P}}$ represented by ω_{r}.

When the WT uses an adaptive frequency-regulation scheme for frequency support, $P_{\mathrm{ref,P}}(\omega_{\mathrm{r,min}})=P_{\mathrm{MPPT}}(\omega_{\mathrm{r},0})$ when ω_{r} is reduced to $\omega_{\mathrm{r,min}}$. However, because the mechanical power P_{m} of the WT decreases as ω_{r} decreases, $P_{\mathrm{ref,P}}(\omega_{\mathrm{r,min}})$ is greater than $P_{\mathrm{m}}(\omega_{\mathrm{r,min}})$. Furthermore, if the power reference value jumps from $P_{\mathrm{ref,P}}(\omega_{\mathrm{r,min}})$ to $P_{\mathrm{m}}(\omega_{\mathrm{r,min}})$ to start rotational speed recovery [37], the electromagnetic power of the WT cannot step due to the PI response speed limit. If $P_{\mathrm{ref,P}}$ remains greater than P_{m} for an extended period, the WT rotational speed decreases until it stops.

Thus, a power-buffer interval is used to strike a balance between the demands of efficient frequency support and safe rotational speed recovery of the WT.

Figure 4 shows the active power of the WT during the frequency-regulation stage, where $P_{\mathrm{ref,P},i}(\omega_{\mathrm{r}})$ and $P_{\mathrm{MPPT}}(v_i)$ are the active power reference and optimal power, respectively, corresponding to the wind speed v_i $(i=0,1,2,3)$. The suffix ω_{r} indicates that the power references change with ω_{r}.

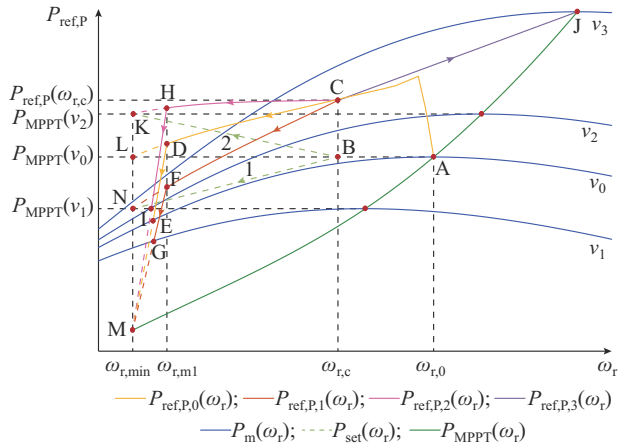

Fig. 4. Active power of WT during frequency-regulation stage.

Before ω_{r} decreases to $\omega_{\mathrm{r,m1}}$, the WT uses an adaptive frequency-support scheme, which corresponds to curve A-C-D. This ensures that the WT can provide sufficient power support for onshore AC systems in the high-rotational speed region. To prevent WT from stalling due to the power step, $P_{\mathrm{ref,P}}$ is moved along curve DM to the intersection E of curve DM and $P_{\mathrm{m}}(v_0)$ when ω_{r} decreases to $\omega_{\mathrm{r,m1}}$, prompting the WT to smoothly switch from frequency support to rotational speed recovery. $P_{\mathrm{ref,P}}$ during DE is expressed as:

$$P_{\mathrm{ref,P}}=P_{\mathrm{MPPT}}(\omega_{\mathrm{r,min}})+\frac{P_{\mathrm{ref,P}}(v_0,\omega_{\mathrm{r,m1}})-P_{\mathrm{MPPT}}(\omega_{\mathrm{r,min}})}{\omega_{\mathrm{r,m1}}-\omega_{\mathrm{r,min}}}(\omega_{\mathrm{r}}-\omega_{\mathrm{r,min}}) \tag{14}$$

When ω_{r} decreases to $\omega_{\mathrm{r,c}}$, the wind speed changes abruptly; subsequently, the frequency-support scheme must be adjusted. If the wind speed is v_1, and v_1 is less than v_0, P_{m} of the WT is represented by the blue curve corresponding to v_1 in Fig. 4. If $P_{\mathrm{ref,P}}$ still moves along curve CD, ω_{r} is likely to decrease rapidly, causing a stall. Thus, $P_{\mathrm{set}}(\omega_{\mathrm{r}})$ should transition from $P_{\mathrm{MPPT}}(\omega_{\mathrm{r},0})$ to $P_{\mathrm{MPPT}}(v_1,\omega_{\mathrm{r,opt},1})$ along the dotted curve BN.

$$P_{\mathrm{set}}(\omega_{\mathrm{r}})=\varepsilon P_{\mathrm{MPPT}}(\omega_{\mathrm{r},0})+(1-\varepsilon)P_{\mathrm{MPPT}}(v_1,\omega_{\mathrm{r,opt},1}) \tag{15}$$

where $\omega_{\mathrm{r,opt},1}$ is the optimal rotational speed corresponding to v_1. The transmit factor ε is expressed as:

$$\varepsilon=\frac{\omega_{\mathrm{r}}-\omega_{\mathrm{r,min}}}{\omega_{\mathrm{r,c}}-\omega_{\mathrm{r,min}}} \tag{16}$$

When the wind speed suddenly changes to v_1, $P_{\mathrm{ref,P}}$ runs along curve CN to point F and then along curve FM to point G according to (14).

Although P_{m} of the WT increases when the wind speed suddenly changes to v_2, $P_{\mathrm{ref,P}}(\omega_{\mathrm{r,c}})$ remains greater than $P_{\mathrm{m}}(v_2,\omega_{\mathrm{r,c}})$ at this time, and the WT rotational speed can continue to decrease to provide frequency support. If the WT still uses $P_{\mathrm{ref,P}}$ at v_0, the increase of mechanical power generated by the increase of wind speed cannot be effectively utilized. Subsequently, along the dashed curve BK, the transition $P_{\mathrm{set}}(\omega_{\mathrm{r}})$ from $P_{\mathrm{MPPT}}(\omega_{\mathrm{r},0})$ to $P_{\mathrm{MPPT}}(v_2,\omega_{\mathrm{r,opt},2})$ occurs. Thus, $P_{\mathrm{ref,P}}$ follows the curve CK to point H and then along the curve HM to point I.

When the wind speed becomes v_3, $P_{\mathrm{ref,P}}(\omega_{\mathrm{r,c}})$ is smaller than $P_{\mathrm{m}}(v_3,\omega_{\mathrm{r,c}})$, and the WT can no longer release kinetic energy by slowing down. However, as the primary goal of WT frequency support is to increase electromagnetic power rather than reduce rotational speed, the power increase and rotational speed recovery are accomplished concurrently along the curve CJ of $P_{\mathrm{ref,P}}(\omega_{\mathrm{r}})$.

$$P_{\mathrm{ref,P}}(\omega_{\mathrm{r}})=P_{\mathrm{ref,P}}(\omega_{\mathrm{r,c}})+\frac{P_{\mathrm{MPPT}}(v_3,\omega_{\mathrm{r,opt},3})-P_{\mathrm{ref,P}}(\omega_{\mathrm{r,c}})}{\omega_{\mathrm{r,opt},3}-\omega_{\mathrm{r,c}}}(\omega_{\mathrm{r}}-\omega_{\mathrm{r,c}}) \tag{17}$$

where $\omega_{\mathrm{r,opt},3}$ is the optimal rotational speed corresponding to v_3.

The adaptive equivalent damping and inertia coefficients comprehensively consider the frequency-regulation demand of the onshore AC system and feedback of the real-time frequency-regulation capacity of the WT, balancing frequency support and rotational speed stability. The power buffer interval prevents the WT from stalling due to the power step. During the frequency-regulation stage, the fundamental active power-tuning approach improves the adaptability of the WT to different wind speeds and makes full use of frequency-regulation resources.

C. WT Rotational Speed Recovery Scheme

Assume that the WT rotational speed is restored from point D in Fig. 5, where $P_{\mathrm{rec},0}(\omega_{\mathrm{r}})$ and $P_{\mathrm{rec},2}(\omega_{\mathrm{r}})$ are the active power references corresponding to wind speeds v_0 and v_2 during the restoration stage, respectively. $P_{\mathrm{rec},1,i}(\omega_{\mathrm{r}})$ is the active power of different scenarios corresponding to wind speed v_1 during the restoration stage ($i=1, 2, 3$). $P_{\mathrm{sec}}(\omega_{\mathrm{r}})$ is the transitional power during the restoration stage.

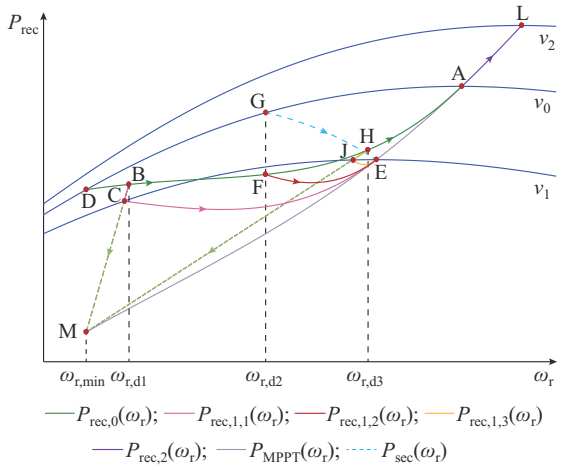

Fig. 5. Active WT power during restoration stage.

If the wind speed remains v_0, $\gamma(v_0)$ is defined as:

$$\gamma(v_0)=\frac{\omega_{\mathrm{r}}-\omega_{\mathrm{r,d}}}{\omega_{\mathrm{r},0}-\omega_{\mathrm{r,d}}} \tag{18}$$

where $\omega_{\mathrm{r,d}}$ is the rotational speed at point D. The electromagnetic power reference value P_{rec} during the restoration stage is set as:

$$P_{\mathrm{rec}}=(1-\gamma(v_0))P_{\mathrm{sec}}(v_0,\omega_{\mathrm{r}})+\gamma(v_0)P_{\mathrm{MPPT}}(\omega_{\mathrm{r}}) \tag{19}$$

where $P_{\mathrm{sec}}(v_0,\omega_{\mathrm{r}})=P_{\mathrm{m}}(v_0,\omega_{\mathrm{r}})$, and $P_{\mathrm{m}}(v_0,\omega_{\mathrm{r}})$ is calculated by [11].

However, the electromagnetic power and mechanical power are equal at point D and the WT does not activate rotational speed recovery [37]. Thus, we multiply (19) by a driving factor τ.

$$P_{\mathrm{rec}}=((1-\gamma(v_0))P_{\mathrm{sec}}(v_0,\omega_{\mathrm{r}})+\gamma(v_0)P_{\mathrm{MPPT}}(\omega_{\mathrm{r}}))\tau \tag{20}$$

τ is defined as:

$$\tau=0.98+\frac{0.02}{\omega_{\mathrm{r,m1}}-\omega_{\mathrm{r,d}}}(\omega_{\mathrm{r}}-\omega_{\mathrm{r,d}}) \tag{21}$$

Using the rotational speed recovery scheme in (18)-(21), the WT starts from point D, follows curve D-B-F-H-A, progressively approaches the MPPT curve, and eventually runs stably at the initial operating point A.

Furthermore, when the wind speed changes from v_0 to v_1, three cases may occur during the restoration stage. In the first case, when the WT runs to point B, the wind speed suddenly changes to v_1. At this point, the electromagnetic power of the WT is greater than its mechanical power. This results in a new reduction in rotational speed. Referring to the electromagnetic power change approach in (14), let P_{rec} run along curve BM to point C, then restart speed recovery at point C using (19), converging to point E of the MPPT curve corresponding to v_1 along the curve CE. The curve B-C-E is described as follows.

$$P_{\mathrm{rec}}=\begin{cases}P_{\mathrm{MPPT}}(\omega_{\mathrm{r,min}})+\dfrac{P_{\mathrm{rec}}(v_0,\omega_{\mathrm{r,d1}})-P_{\mathrm{MPPT}}(\omega_{\mathrm{r,min}})}{\omega_{\mathrm{r,d1}}-\omega_{\mathrm{r,min}}}(\omega_{\mathrm{r}}-\omega_{\mathrm{r,min}}) & \dfrac{\mathrm{d}\omega_{\mathrm{r}}}{\mathrm{d}t}<0\\ (1-\gamma(v_1))P_{\mathrm{m}}(v_1,\omega_{\mathrm{r}})+\gamma(v_1)P_{\mathrm{MPPT}}(\omega_{\mathrm{r}}) & \dfrac{\mathrm{d}\omega_{\mathrm{r}}}{\mathrm{d}t}>0\end{cases} \tag{22}$$

$\gamma(v_1)$ is defined as:

$$\gamma(v_1)=\frac{\omega_{\mathrm{r}}-\omega_{\mathrm{r,d1}}}{\omega_{\mathrm{r,opt,1}}-\omega_{\mathrm{r,d1}}} \tag{23}$$

In the second case, the WT encounters a sudden change of wind speed at point F. At this time, the mechanical power corresponding to v_1 exceeds the electromagnetic power, and the WT is still able to recover its rotational speed. However, due to the environment change, P_{rec} is modified in conjunction with the design principle of P_{set}. $\gamma(\omega_{\mathrm{r}})$ transitions from v_0 to v_1.

$$\gamma(\omega_{\mathrm{r}})=\gamma(v_0,\omega_{\mathrm{r,d2}})+\frac{1-\gamma(v_0,\omega_{\mathrm{r,d2}})}{\omega_{\mathrm{r,opt,1}}-\omega_{\mathrm{r,d2}}}(\omega_{\mathrm{r}}-\omega_{\mathrm{r,d2}}) \tag{24}$$

$P_{\mathrm{sec}}(\omega_{\mathrm{r}})$ transitions from $P_{\mathrm{m}}(v_0)$ to $P_{\mathrm{m}}(v_1)$ along GE as:

$$P_{\mathrm{sec}}(\omega_{\mathrm{r}})=(1-\mu)P_{\mathrm{m}}(v_0,\omega_{\mathrm{r}})+\mu P_{\mathrm{m}}(v_1,\omega_{\mathrm{r}}) \tag{25}$$

μ is defined as:

$$\mu=\frac{\omega_{\mathrm{r}}-\omega_{\mathrm{r,d2}}}{\omega_{\mathrm{r,opt,1}}-\omega_{\mathrm{r,d2}}} \tag{26}$$

The WT moves along the curve D-B-F-E, described as:

$$P_{\mathrm{rec}}(\omega_{\mathrm{r}})=(1-\gamma(\omega_{\mathrm{r}}))P_{\mathrm{sec}}(\omega_{\mathrm{r}})+\gamma(\omega_{\mathrm{r}})P_{\mathrm{MPPT}}(\omega_{\mathrm{r}}) \tag{27}$$

In the third case, the wind speed changes at point H, and (22) is used to make the WT run along curve HM to point J and subsequently restore the rotational speed along curve JE.

When the wind speed changes from v_0 to v_2, the rotational speed is recovered according to (20). When the WT reaches point A, P_{rec} converges to point L along the MPPT curve, corresponding to the curve D-B-F-H-A-L.

The rotational speed recovery scheme used in this study gradually transitions from the P_{m} curve to the MPPT curve. Under this setting, the power fluctuation at the starting point is small. P_{rec} is kept high during the restoration stage to avoid further deterioration of the AC system frequency. The control mode of P_{rec} guarantees that the WT is able to successfully complete rotational speed recovery in different wind speeds, compensating for the WT rotational speed recovery that does not consider the changes of wind speed.

D. Hierarchical Zoning Frequency-regulation Scheme

Due to lacking a comprehensive framework for an auxiliary frequency-regulation scheme for VSC-MTDC systems with wind farms, a hierarchical zoning frequency-regulation scheme based on local autonomy and global cooperation is proposed.

In this context, the frequency response of a disturbed AC system is determined mainly by the generators. To avoid the influence of minor frequency disturbances on the other VSCs, a frequency deadband is set for the GSVSC. Thus, (1) can be modified as:

$$\Delta P_{\mathrm{ref,G}} = -\frac{1}{K_{\mathrm{V}}}\Delta U_{\mathrm{dc}} + K_{\mathrm{f}}\Delta f_{\mathrm{G}} \tag{28}$$

where $\Delta P_{\mathrm{ref,G}} = P_{\mathrm{ref,G}} - P_{\mathrm{G}}$. Δf_{G} is given as:

$$\Delta f_{\mathrm{G}} = \begin{cases} 0 & \left|\Delta f_{\mathrm{G},0}\right| < \Delta f_{\mathrm{mar}} \\ \Delta f_{\mathrm{G},0} - \mathrm{sign}(\Delta f_{\mathrm{G},0})\Delta f_{\mathrm{mar}} & \left|\Delta f_{\mathrm{G},0}\right| \geq \Delta f_{\mathrm{mar}} \end{cases} \tag{29}$$

where the actual frequency deviation of the disturbed AC system is $\Delta f_{\mathrm{G},0} = f^{*} - f$; Δf_{mar} is the frequency deadband, usually $\Delta f_{\mathrm{mar}} = 0.05$ Hz [33]; and sign(·) represents the symbol function.

When the FE of the disturbed AC system exceeds Δf_{mar}, under the actions of (1) and (28), the FE is directly related to the DC voltage; thus, the capacitor energy storage E_{dc} of the DC grid is used to provide short-term frequency support. E_{dc} is expressed as:

$$E_{\mathrm{dc}} = \frac{1}{2}C_{\mathrm{eq}}U_{\mathrm{dc}}^{2} \tag{30}$$

where C_{eq} is the equivalent capacitance of the MMC.

E_{dc} varies by approximately 4% when U_{dc} varies by 2% from the rated operating state. The critical DC voltage with a limit of 0.02 p.u. can use the DC capacitor energy storage to provide frequency support and does not cause the DC voltage to deviate greatly, which can threaten the safety of the DC system.

The frequency of an offshore AC system is coupled with the DC voltage using (2). The first type of DC voltage deadband $\Delta U_{\mathrm{dcmar1}}$ is set similar to the frequency deadband such that the wind farm began frequency support when the DC voltage exceeds $\Delta U_{\mathrm{dcmar1}}$. ΔU_{dc} in (2) is modified as $\Delta U_{\mathrm{dc,W1}}$:

$$\Delta U_{\mathrm{dc,W1}} = \begin{cases} 0 & \left|\Delta U_{\mathrm{dc}}\right| < \Delta U_{\mathrm{dcmar1}} \\ \Delta U_{\mathrm{dc}} - \mathrm{sign}(\Delta U_{\mathrm{dc}})\Delta U_{\mathrm{dcmar1}} & \left|\Delta U_{\mathrm{dc}}\right| \geq \Delta U_{\mathrm{dcmar1}} \end{cases} \tag{31}$$

Figure 6 shows the frequency-conversion control with the deadband of the WFVSC. Because there are multiple wind farms in an MTDC system, it is necessary to partition the wind farms to provide a sequential frequency-regulation service. According to the frequency-support capacity coefficients $G_{\mathrm{C,WF}}$, the wind farms are categorized into two types. The first 50% are used for priority frequency-support after ΔU_{dc} exceeds $\Delta U_{\mathrm{dcmar1}}$; and the remaining 50% are used when the first type of wind farms had an insufficient support capacity. Wind farms with large capacities are chosen for priority frequency support when the values of $G_{\mathrm{C,WF}}$ are similar.

In the first type of wind farms, if the frequency of the disturbed AC system stabilizes, the frequency-regulation service is terminated in advance, and the rotational speed is restored.

$$\begin{cases} \dfrac{\mathrm{d}\omega_{\mathrm{r}}}{\mathrm{d}t} < 0 \\ \dfrac{\mathrm{d}f_{\mathrm{owf}}}{\mathrm{d}t} = 0 \end{cases} \tag{32}$$

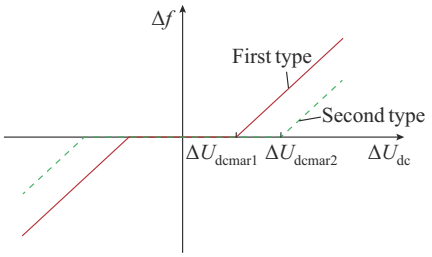

Fig. 6. Frequency-conversion control with deadband of WFVSC.

At this time, the second type of wind farms begin frequency support to compensate for the SFD induced by the power drop of the first type. Furthermore, when ω_{r} of the first type fall to $\omega_{\mathrm{r,m1}}$, the wind farms enter the power-buffer interval and their output power greatly decreases. The second type of wind farms must also be activated. Thus, the intervention conditions for the second type of wind farms are:

$$\Delta U_{\mathrm{dc,W2}} = \begin{cases} 0 & \left|\Delta U_{\mathrm{dc}}\right| < \Delta U_{\mathrm{dcmar2}} \\ \Delta U_{\mathrm{dc}} - \mathrm{sign}(\Delta U_{\mathrm{dc}})\Delta U_{\mathrm{dcmar2}} & \left|\Delta U_{\mathrm{dc}}\right| \geq \Delta U_{\mathrm{dcmar2}} \end{cases} \tag{33}$$

where $\Delta U_{\mathrm{dcmar2}}$ is the DC voltage deviation of the WFVSC connected to the second type of wind farms when the first type satisfies the termination conditions.

Whether the second type of wind farms provide frequency support for a disturbed AC system or compensates for the power deficit caused by the rotational speed recovery of the first type, they must continue to support power until their frequency-regulation resources are exhausted. Thus, the termination conditions for the second type of wind farms are:

$$\omega_{\mathrm{r}} = \omega_{\mathrm{r,m1}} \tag{34}$$

To preferentially utilize the DC capacitor energy storage and kinetic energy of the WT during the early frequency-regulation stage, the GSVSCs connected to normal AC systems are converted from droop control to fixed-power control. When the second type of wind farms met the termination condition, the normal GSVSCs restart the droop control to continue regulating the frequency or provide power support for WT rotational speed recovery. Thus, normal GSVSCs use DC voltage droop control with a deadband, as shown in Fig. 7, where $U_{\mathrm{dc,0}}$ and $P_{\mathrm{G,0}}$ are the initial values of the DC voltage and active power of the normal VSC, respectively; and $U_{\mathrm{dc,1}}$ is the activated DC voltage of a normal GSVSC.

A control block diagram of the hierarchical partitioned frequency-regulation scheme is presented in Fig. 8.

When a power supply-demand imbalance emerges in an onshore AC system, the generators begin frequency regulation. If the regulation capacity of a disturbed AC system is insufficient, DC capacitor energy storage is preferred for frequency support. If the frequency deteriorates further, the two types of wind farms provide frequency support according to their respective frequency-regulation capabilities. After fre-

quency support provided by the wind farms, the VSCs connected to the normal AC system use droop control to share the unbalanced power caused by the rotational speed recovery of the WT to ameliorate multiple frequency dips.

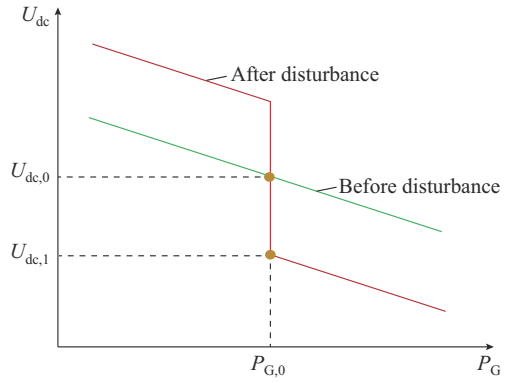

Fig. 7. Control strategy of normal GSVSC.

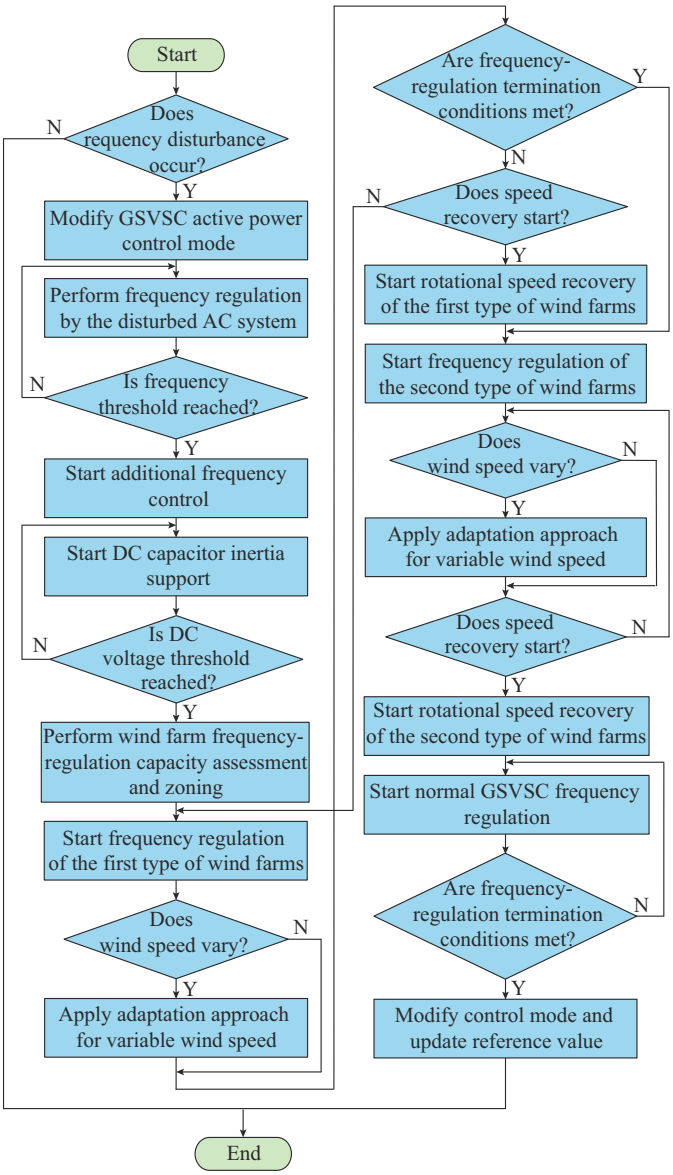

Fig. 8. Control block diagram of hierarchical partitioned frequency-regulation scheme.

E. Small-signal Stability Analysis

To study the stability of K_D and K_i of the VIIC, a frequency stability analysis model including the PMSG machine-side converter and the WFVSC has been established using a small-signal model of the VSC [38]. The detailed small-signal analysis model and control parameters are presented in Appendix A Fig. A1 and Table AI. The analysis results are presented in Fig. 9.

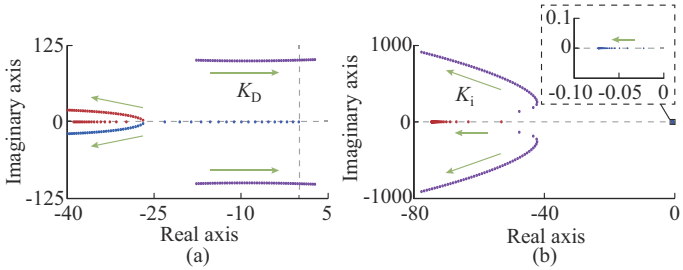

Fig. 9. Small-signal stability analysis results for K_D and K_i. (a) Root locus of K_D from 0 to 50. (b) Root locus of K_i from 0 to 50.

In Fig. 9(a), as K_D increases from 0 to 50, a pair of eigenvalues crosses the imaginary axis and enters an unstable state. The critical value of K_D is 42.5, which far exceeds its normal value. Moreover, when K_i increases from 0 to 50, all eigenvalues move to the left of the imaginary axis in Fig. 9(b), indicating that there is no stability concern. The small-signal stability study in Fig. 9 demonstrate that within the normal parameter range, VIIC does not affect stable operation of the WT.

IV. Simulations

A simulation model of the VSC-MTDC system shown in Fig. 1 has been built using PSCAD/EMTDC to validate the efficiency of the cooperative frequency-regulation scheme. The simulation model parameters are presented in Appendix A Table AII.

A. Verification of WT Adaptive Frequency-regulation Scheme

1) Slight Power Disturbance Verification

When $t=15$ s, the load of AC system 3 (AC_3) suddenly increases by 50 MW, and only wind farm 1 (WF_1) is engaged in frequency regulation; $v=10$ m/s. Mode 1 is the scheme used in this paper. Mode 2 is the strategy without frequency support, and Mode 3 is the approach used in [39]. The simulation results are depicted in Fig. 10, where f_3 is the frequency of AC_3; and $P_{W,1}$ and $\omega_{r,1}$ are the active power and rotational speed of WF_1, respectively.

In Fig. 10, if no additional frequency-regulation scheme is used, f_3 rapidly decreases to 49.76 Hz. When Mode 3 detects a drop in f_3, $P_{W,1}$ increases from 450 MW to 495 MW to provide frequency support for AC_3. Limited by the response speed of the PI, f_3 stabilizes at 49.94 Hz after slight fluctuation. At $t=45$ s, $\omega_{r,1}$ drops to 0.71 p.u., and Mode 3 starts rotational speed recovery. $P_{W,1}$ gradually drops to 386 MW, causing f_3 to drop to 49.32 Hz, with a significant SFD. Furthermore, $P_{W,1}$ increases to 494 MW after using the adaptive VIIC and decreases when $\omega_{r,1}$ drops. However, f_3 is always greater than 49.87 Hz. Compared with Mode 3, the decrease

does not exceed 0.07 Hz, and the frequency-support time is extended from 30 s to 35 s. The minimum value of f_3 during the restoration stage of Mode 1 is 49.64 Hz, which is 0.32 Hz higher than that in Mode 3. Figure 10 illustrates that the adaptive VIIC maintains a high frequency for an extended time during the early stage of a minor power disturbance, seeking time for subsequent frequency regulation.

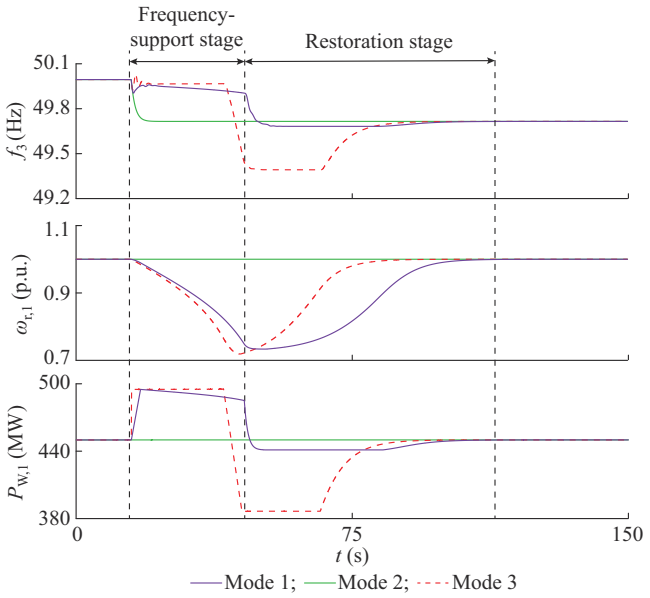

Fig. 10. Frequency-regulation results with a small power disturbance.

2) Large Power Disturbance Verification

At $t=15$ s, the load of AC_3 suddenly increases by 100 MW; and the other conditions remain unchanged.

Relying only on the frequency-regulation capacity of AC_3, f_3 rapidly drops to 49.52 Hz, as shown in Fig. 11. Mode 3 increases $P_{W,1}$ by 45 MW to achieve frequency regulation, and f_3 increases to 49.74 Hz. During the restoration stage, the minimum f_3 of Mode 3 is 49.21 Hz. However, Mode 1 rapidly increases $P_{W,1}$ to 540 MW when the AC_3 load changes substantially, and the decline in f_3 is significantly reduced. With the release of kinetic energy from the WT, the power support provided by WF_1 gradually decreases to 510 MW, and f_3 remains greater than that in Mode 3. Furthermore, the rotational-speed recovery of Mode 1 is smoother and the minimum f_3 is 0.28 Hz higher than that in Mode 3. Figure 11 shows that when the load variation is large, adaptive VIIC rapidly increases the frequency-support power, and the frequency decline is significantly slowed. The SFD improves substantially during the restoration stage.

B. Verification of WT Power Adaptation Approach

When $t=15$ s, the load of AC_3 suddenly increases by 100 MW; when $t=25$ s, v increases from 10 m/s to 11 m/s; and when $t=60$ s, v decreases to 8.5 m/s.

Due to the change of WF_1 output power induced by the change in v, f_3 in Mode 2 decreases from 50 Hz to 49.52 Hz, then gradually increases to 49.72 Hz, and decreases to 49.11 Hz. Mode 3 maintains $P_{W,1}$ at 495 MW during the frequency-support stage, wasting the potential increase of mechanical power as v increases. However, during the restoration stage, v decreases significantly; the mechanical power of the WT is less than the electromagnetic power, and $\omega_{r,1}$ decreases. To prevent $\omega_{r,1}$ from falling below 0.7 p.u. and causing the WT to stall, Mode 3 should run at 0.7 p.u.. In Mode 1, the reference value of active power is transitioned by (14) at 25 s, such that $P_{W,1}$ increases after v increases, and f_3 increases from 49.86 Hz to 49.96 Hz, considerably improving the frequency state of AC_3. Mode 1 uses (22) to convert P_{rec} after v drops during the restoration stage, and $\omega_{r,1}$ restarts recovery after a slight decline. Figure 12 demonstrates that the adaptation approach to variable wind speeds makes full use of the real-time frequency resources of the WT during the frequency-regulation stage and switches states in time during the restoration stage to effectively avoid the risk of WT stalling.

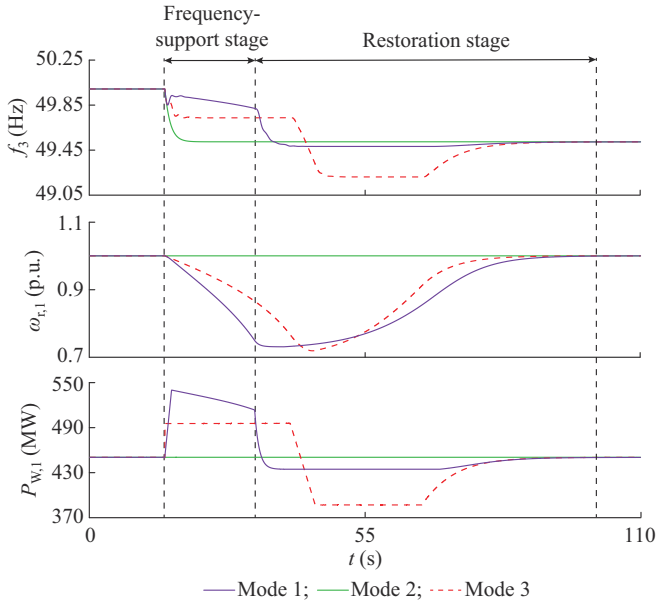

Fig. 11. Frequency-regulation results with a large power disturbance.

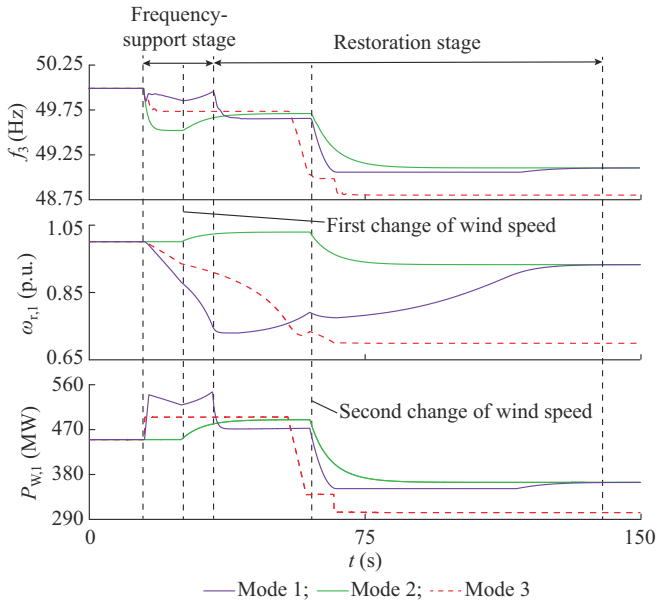

Fig. 12. $WFVSC_1$ frequency-regulation results with variable wind speed.

C. Verification of Cooperative Frequency-regulation Scheme

The load on AC_3 suddenly increases by 100 MW at t=15 s. When t=25 s, v of WF_1 increases from 10 m/s to 11 m/s; when t=60 s, v decreases to 10.5 m/s. When t=34.2 s, v of WF_2 increases from 10 m/s to 11 m/s; when t=79.2 s, v decreases to 10.5 m/s. Mode 4 uses only wind farms for frequency regulation, whereas Mode 5 uses only normal GSVSCs. The simulation results are shown in Fig. 13, where $P_{W,2}$ and $\omega_{r,2}$ are the active power and rotational speed of WF_2, respectively; $P_{G,3}$ and $P_{G,4}$ are the active power of $GSVSC_3$ and $GSVSC_4$, respectively; and $U_{dc,3}$ is the DC voltage of $GSVSC_3$.

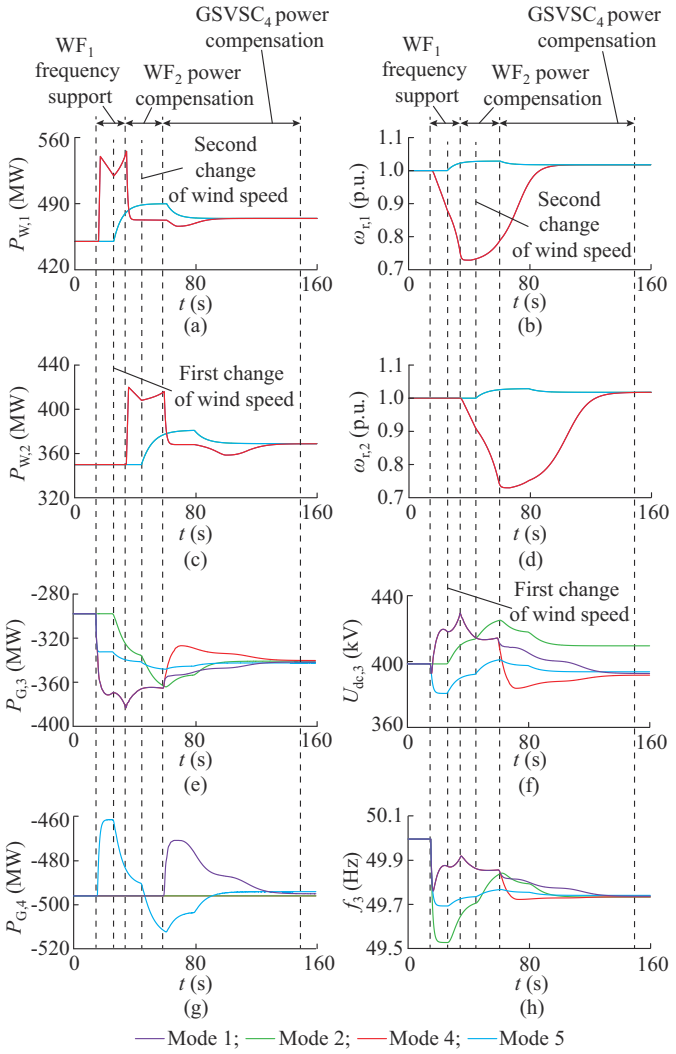

Fig. 13. Simulation results with cooperative frequency-regulation scheme. (a) $P_{W,1}$. (b) $\omega_{r,1}$. (c) $P_{W,2}$. (d) $\omega_{r,2}$. (e) $P_{G,3}$. (f) $U_{dc,3}$. (g) $P_{G,4}$. (h) f_3.

Mode 4 uses WF_2 to compensate for the power shortage generated by WF_1, ensuring that f_3 remains above 49.85 Hz. However, after WF_2 begins to recover, $P_{W,2}$ decreases from 413 MW to 368 MW, causing f_3 to decrease to 49.72 Hz and $U_{dc,3}$ to decrease to 383 kV. Although WF_2 improves the SFD of WF_1, the third frequency dip (TFD) threatens the stability of the frequency and DC voltage. In Mode 5, $GSVSC_4$ shares unbalanced power through droop control. After f_3 decreases from 50 Hz to 49.68 Hz, it fluctuates slightly with the changes of wind speed of WF_1 and WF_2. After Mode 1 detects a frequency drop, WF_1 uses an adaptive VIIC to quickly implement power support such that f_3 is maintained above 49.75 Hz. Furthermore, consistent with Mode 4, WF_2 improves the SFD of WF_1. $GSVSC_4$ is activated by the cooperative frequency-regulation scheme to compensate for the power deficiency when WF_2 performs rotational speed recovery. Compared with Mode 4, the deviations of f_3 and $U_{dc,3}$ decrease, and the TFD is significantly improved. Cooperative frequency-regulation scheme uses the first type of wind farms for high-quality frequency support, alleviates the SFD with the second type of wind farms, and prevents severe TFD with normal GSVSCs.

V. Conclusion

This paper proposes a novel frequency-regulation scheme for VSC-MTDC system with offshore wind farms to address the problems of insufficient flexibility of the VIIC of WTs and poor adaptability of frequency-regulation schemes to the changes of wind speed.

1) The adaptive frequency-regulation control dynamically adjusts the WT support power according to the system frequency status and frequency-regulation capacity of the WT. When the system load change is minor, adaptive VIIC provides appropriate power support and effectively extends the WT frequency-support time. Power disturbances are fully supported when the system load changes drastically, which significantly improves frequency stability during the early stages of a power disturbance.

2) The power adaptation technique at variable wind speeds dynamically adjusts the basic power and fully utilizes the frequency-regulation resources of the WT during the frequency-support stage. During the restoration stage, the WT power should be reasonably changed to successfully complete rotational speed recovery and prevent WT stalls resulting from excessive wind speed drops.

3) The hierarchical partitioned frequency-regulation scheme uses a step frequency-support sequence that fully utilizes the frequency-regulation potential of each link in the VSC-MTDC system. The sequential frequency-regulation scheme provides outstanding regulation performance and reduces the SFD caused by the first type of wind farm. The participation of normal GSVSCs prevents a TFD during the restoration stage of the second type of wind farms.

Appendix A

A frequency response model of the PMSG machine-side converter and WFVSC is developed based on [38] to analyze the small-signal stability, as shown in Fig. A1, where P_p is the active power of PMSG; and u_{d0} and U_{dc0} are the linearized initial values of u_d and U_{dc}, respectively.

Parameters of frequency stability analysis model are listed in Table AI.

The parameters of the simulation model are listed in Table AII.

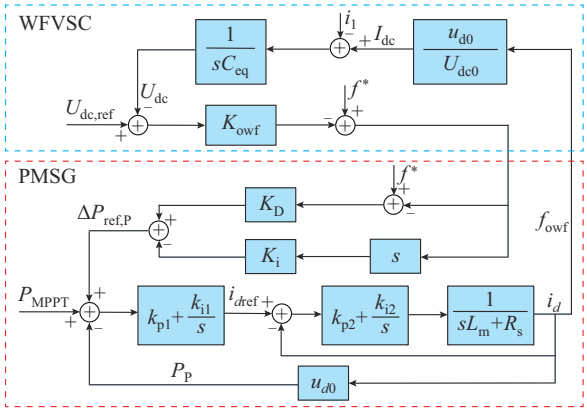

Fig. A1. Frequency stability analysis model of PMSG integrated to power grid via WFVSC.

TABLE AI
PARAMETERS OF FREQUENCY STABILITY ANALYSIS MODEL

Symbol	Definition	Value
$U_{dc,ref}$	DC voltage reference value	400 kV
f^*	AC system frequency reference value	50 Hz
C_{eq}	Equivalent DC capacitance of MMC	1800 μF
K_{owf}	Frequency-conversion coefficient of WFVSC	1 p.u.
K_D	Equivalent damping coefficient	1.5 p.u.
K_i	Equivalent inertia coefficient	1.8 p.u.
k_{p1}	Proportional coefficient of *d*-axis outer-loop of machine-side converter of PMSG	0.01 p.u.
k_{i1}	Integral coefficient of *d*-axis outer-loop of machine-side converter of PMSG	100 p.u.
k_{p2}	Proportional coefficient of *d*-axis inner-loop of machine-side converter of PMSG	0.5 p.u.
k_{i2}	Integral coefficient of *d*-axis inner-loop of machine-side converter of PMSG	100 p.u.
R_s	Equivalent AC resistance of machine-side converter of PMSG	0.3142 Ω
L_m	Equivalent AC inductance of machine-side converter of PMSG	0.021 H

TABLE AII
PARAMETERS OF SIMULATION MODEL

Symbol	Definition	Value
$U_{ac,ref}$	AC voltage reference value	220 kV
$P_{ref,P,1}$	Active power reference value of $WFVSC_1$	450 MW
$P_{ref,P,2}$	Active power reference value of $WFVSC_2$	350 MW
$P_{ref,G,3}$	Active power reference value of $GSVSC_3$	–300 MW
$P_{ref,G,4}$	Active power reference value of $GSVSC_4$	–500 MW
$K_{V,3}$	DC voltage droop coefficient of $GSVSC_3$	0.6667 p.u.
$K_{V,4}$	DC voltage droop coefficient of $GSVSC_4$	0.4 p.u.
P_N	Rated power of single WT	5 MW
$N_{W,1}$	Number of WTs of wind farm connected to $WFVSC_1$	90
$N_{W,2}$	Number of WTs of wind farm connected to $WFVSC_2$	70

REFERENCES

[1] R. Yang, G. Shi, X. Cai *et al.*, "Autonomous synchronizing and frequency response control of multi-terminal DC systems with wind farm integration," *IEEE Transactions on Sustainable Energy*, vol. 11, no. 4, pp. 2504-2514, Oct. 2020.

[2] Z. Li, Z. Wei, R. Zhan *et al.*, "Frequency support control method for interconnected power systems using VSC-MTDC," *IEEE Transactions on Power Systems*, vol. 36, no. 3, pp. 2304-2313, May 2021.

[3] R. Hemmati, H. Mehrjerdi, M. Shafie-khah *et al.*, "Managing multi-type capacity resources for frequency regulation in unit commitment integrated with large wind ramping," *IEEE Transactions on Sustainable Energy*, vol. 12, no. 1, pp. 705-714, Jan. 2021.

[4] M. Mehrabankhomartash, M. Saeedifard, and A. Yazdani, "Adjustable wind farm frequency support through multi-terminal HVDC grids," *IEEE Transactions on Sustainable Energy*, vol. 12, no. 2, pp. 1461-1472, Apr. 2021.

[5] J. Boyle, T. Littler, S. M. Muyeen *et al.*, "An alternative frequency-droop scheme for wind turbines that provide primary frequency regulation via rotor speed control," *International Journal of Electrical Power & Energy Systems*, vol. 133, pp. 1-13, Dec. 2021.

[6] P. Mahish and A. K. Pradhan, "Distributed synchronized control in grid integrated wind farms to improve primary frequency regulation," *IEEE Transactions on Power Systems*, vol. 35, no. 1, pp. 362-373, Jan. 2020.

[7] R. Prasad and N. P. Padhy, "Synergistic frequency regulation control mechanism for DFIG wind turbines with optimal pitch dynamics," *IEEE Transactions on Power Systems*, vol. 35, no. 4, pp. 3181-3191, Jul. 2020.

[8] J. Ouyang, M. Pang, M. Li *et al.*, "Frequency control method based on the dynamic deloading of DFIGs for power systems with high-proportion wind energy," *International Journal of Electrical Power & Energy Systems*, vol. 128, pp. 704-714, Jun. 2021.

[9] G. G. Platero, M. G. Casado, M. P. García *et al.*, "CECRE: supervision and control of Spanish renewable energies in the last 15 years," *Journal of Modern Power Systems and Clean Energy*, vol. 10, no. 2, pp. 269-276, Mar. 2022.

[10] A. Nakamura, F. Alsharif, A. Umemura *et al.*, "Voltage control and virtual synchronous generator control of HVDC interconnection line for improving stability of power system including large-scale wind farm," *IET Generation, Transmission & Distribution*, vol. 15, no. 24, pp. 3375-3387, Dec. 2021.

[11] W. Zhang, W. Sheng, Q. Duan *et al.*, "Automatic generation control with virtual synchronous renewables," *Journal of Modern Power Systems and Clean Energy*, vol. 11, no. 1, pp. 267-279, Jan. 2023.

[12] J. van de Vyver, J. D. M. de Kooning, B. Meersman *et al.*, "Droop control as an alternative inertial response strategy for the synthetic inertia on wind turbines," *IEEE Transactions on Power Systems*, vol. 31, no. 2, pp. 1129-1138, Mar. 2016.

[13] Y. Wu, W. Yang, Y. Hu *et al.*, "Frequency regulation at a wind farm using time-varying inertia and droop controls," *IEEE Transactions on Industry Applications*, vol. 55, no. 1, pp. 213-224, Feb. 2019.

[14] M. Garmroodi, G. Verbič, and D. J. Hill, "Frequency support from wind turbine generators with a time-variable droop characteristic," *IEEE Transactions on Sustainable Energy*, vol. 9, no. 2, pp. 676-684, Apr. 2018.

[15] D. Yang, Z. Jin, T. Zheng *et al.*, "An adaptive droop control strategy with smooth rotor speed recovery capability for type III wind turbine generators," *International Journal of Electrical Power & Energy Systems*, vol. 135, pp. 1-10, Feb. 2022.

[16] Y. Li, Z. Xu, J. Østergaard *et al.*, "Coordinated control strategies for offshore wind farm integration via VSC-HVDC for system frequency support," *IEEE Transactions on Energy Conversion*, vol. 32, no. 3, pp. 843-856, Sept. 2017.

[17] H. Lao, L. Zhang, T. Zhao *et al.*, "Innovated inertia control of DFIG with dynamic rotor speed recovery," *CSEE Journal of Power and Energy Systems*, vol. 8, no. 5, pp. 1417-1427, Sept. 2022.

[18] P. Verma, Seethalekshmi K., and B. Dwivedi, "A cooperative approach of frequency regulation through virtual inertia control and enhancement of low voltage ride-through in DFIG-based wind farm," *Journal of Modern Power Systems and Clean Energy*, vol. 10, no. 6, pp. 1519-1530, Nov. 2022.

[19] J. Lee, E. Muljadi, P. Srensen *et al.*, "Releasable kinetic energy-based inertial control of a DFIG wind power plant," *IEEE Transactions on Sustainable Energy*, vol. 7, no. 1, pp. 279-288, Apr. 2016.

[20] Y. Xiong, W. Yao, J. Wen *et al.*, "Two-level combined control scheme of VSC-MTDC integrated offshore wind farms for onshore system frequency support," *IEEE Transactions on Power Systems*, vol. 36, no. 1, pp. 781-792, Jan. 2021.

[21] Z. Lu, Y. Ye, and Y. Qiao, "An adaptive frequency regulation method with grid-friendly restoration for VSC-HVDC integrated offshore wind farms," *IEEE Transactions on Power Systems*, vol. 34, no. 5, pp. 3582-

3593, Sept. 2019.
[22] D. Ochoa and S. Martinez, "Fast-frequency response provided by DFIG-wind turbines and its impact on the grid," *IEEE Transactions on Power Systems*, vol. 32, no. 5, pp. 4002-4011, Sept. 2017.
[23] Y. Tan, K. M. Muttaqi, P. Ciufo *et al*., "Enhanced frequency regulation using multilevel energy storage in remote area power supply systems," *IEEE Transactions on Power Systems*, vol. 34, no. 1, pp. 163-170, Jan. 2019.
[24] T. Rahimi, L. Ding, M. Kheshti *et al*., "Inertia response coordination strategy of wind generators and hybrid energy storage and operation cost-based multi-objective optimizing of frequency control parameters," *IEEE Access*, vol. 9, pp. 74684-74702, May 2021.
[25] N. R. Ullah, T. Thiringer, and D. Karlsson, "Temporary primary frequency control support by variable speed wind turbines-potential and applications," *IEEE Transactions on Power Systems*, vol. 23, no. 2, pp. 601-612, May 2008.
[26] F. Liu, Z. Liu, S. Mei *et al*., "ESO-based inertia emulation and rotor speed recovery control for DFIGs," *IEEE Transactions on Energy Conversion*, vol. 32, no. 3, pp. 1209-1219, Sept. 2017.
[27] K. Liu, Y. Qu, H. Kim *et al*., "Avoiding frequency second dip in power unreserved control during wind power rotational speed recovery," *IEEE Transactions on Power Systems*, vol. 33, no. 3, pp. 3097-3106, May 2018.
[28] D. Yang, H. Gao, L. Zhang *et al*., "Short-term frequency support of a doubly-fed induction generator based on an adaptive power reference function," *International Journal of Electrical Power & Energy Systems*, vol. 119, pp. 1-10, Jul. 2020.
[29] J. N. Sakamuri, M. Altin, A. D. Hansen *et al*., "Coordinated frequency control from offshore wind power plants connected to multi terminal DC system considering wind speed variation," *IET Renewable Power Generation*, vol. 11, no. 8, pp. 1226-1236, Jun. 2017.
[30] G. Lu, C. Lin, and Y. Wu, "Comparison of communication-based and coordination-based frequency control schemes for HVDC-connected offshore wind farms," *IEEE Transactions on Industry Applications*, vol. 57, no. 4, pp. 3352-3365, Jul. 2021.
[31] M. M. Kabsha and Z. H. Rather, "A new control scheme for fast frequency support from HVDC connected offshore wind farm in low-inertia system," *IEEE Transactions on Sustainable Energy*, vol. 11, no. 3, pp. 1829-1837, Jul. 2020.
[32] Y. Wen, J. Zhan, C. Y. Chung *et al*., "Frequency stability enhancement of integrated AC/VSC-MTDC systems with massive infeed of offshore wind generation," *IEEE Transactions on Power Systems*, vol. 33, no. 5, pp. 5135-5146, Sept. 2018.
[33] A. Kirakosyan, E. F. E. Saadany, M. S. E. Moursi *et al*., "Selective frequency support approach for MTDC systems integrating wind generation," *IEEE Transactions on Power Systems*, vol. 36, no. 1, pp. 366-378, Jan. 2021.
[34] X. Cao, B. Stephen, I. F. Abdulhadi *et al*., "Switching Markov Gaussian models for dynamic power system inertia estimation," *IEEE Transactions on Power Systems*, vol. 31, no. 5, pp. 3394-3403, Sept. 2016.
[35] W. Zhang, C. Wu, W. Huang *et al*., "Evaluation of system frequency characteristic and parameter setting of frequency regulation for wind power considering secondary frequency drop," *Automation of Electric Power Systems*, vol. 46, no. 8, pp. 11-19, Apr. 2022.
[36] R. Zhao, Y. Wen, X. Ye *et al*., "Research on frequency indicators evaluation of disturbance events based on improved stacked denoising autoencoders," *Proceedings of the CSEE*, vol. 39, no. 14, pp. 4081-4092, Jul. 2019.
[37] M. Kang, E. Muljadi, K. Hur *et al*., "Stable adaptive inertial control of a doubly-fed induction generator," *IEEE Transactions on Smart Grid*, vol. 7, no. 6, pp. 2971-2979, Nov. 2016.
[38] C. Liu, H. Liu, S. Jiang *et al*., "Dynamic frequency support and DC voltage regulation approach for VSC-MTDC systems," *CSEE Journal of Power and Energy Systems*, vol. 9, no. 2, pp. 645-658, Mar. 2023.
[39] S. El Itani, U. D. Annakkage, G. Joos *et al*., "Short-term frequency support utilizing inertial response of DFIG wind turbines," in *Proceeding of 2011 IEEE PES General Meeting*, Detroit, USA, Jul. 2011, pp. 1-8.

Haoyu Liu received the B. S. degree in electrical engineering from North China Electric Power University, Beijing, China, in 2017, where he is currently pursuing the Ph.D. degree. His research interests include coordination control and stability analysis of voltage source converter-based multi-terminal high-voltage direct current (VSC-MTDC).

Chongru Liu received the B.S. and Ph.D. degrees in electrical engineering from Tsinghua University, Beijing, China, in 2000 and 2006, respectively. She was a Visiting Professor at the University of Hong Kong, Hong Kong, China, from 2009 to 2010, and she was a Visiting Professor at Washington State University, Seattle, USA, from 2010 to 2011. She is currently a Professor in the School of Electrical and Electronic Engineering, North China Electric Power University, Beijing, China. She is a Member of the National Power System Management and Information Exchange Standardization Committee of China. She is a Member of Beijing Nova and supported by the program of New Century Excellent Talents in University. Her research interests include analysis, simulation and control of AC/DC hybrid system.